Tuning the topology of a two-dimensional catenated DNA network

Indresh Yadav , ¹ Dana Al Sulaiman , ² and Patrick S. Doyle ¹,*

¹Department of Chemical Engineering, Massachusetts Institute of Technology, Cambridge, Massachusetts 02139, USA ²Division of Physical Science and Engineering, King Abdullah University of Science and Technology, Thuwal 23955-6900, Saudi Arabia

(Received 22 July 2022; accepted 5 January 2023; published 24 February 2023)

Molecular topology of polymers plays a key role in determining their physical properties. We studied herein the topological effects on the static and dynamic properties of a 2D catenated network of DNA rings called a kinetoplast. Restriction enzymes that cleave DNA at sequence-specific sites are used to selectively cut and remove rings from the network and hence tune the molecular topology while maintaining overall structural integrity. We find that topology has minimal effects over the spatial extension of the 2D network; however, it significantly affects the relaxation behavior. The shape fluctuations of the network are governed by two distinct characteristic time scales attributed to the thermal fluctuations and confinement of the network. The relationship between the time constant of thermal relaxation and the amplitude of anisotropy fluctuations yields a universal scaling. Interestingly, this scaling is independent of the detailed arrangements of rings and/or perforation within the catenated networks. This study provides a route to tune the elastic properties of 2D catenated DNA networks and other polymeric materials by modifying the underlying topology in a rational and highly controllable manner.

DOI: 10.1103/PhysRevResearch.5.013141

I. INTRODUCTION

The topology of polymer molecules plays an important role in determining their static (e.g., size and shape) and dynamic (e.g., relaxation and diffusion) properties [1,2]. Tuning the topology of molecules is thus imperative in controlling the physicochemical properties tailored for desired applications [3]. Recently, a class of mechanically interlinked polymers molecules called polycatenanes have received considerable attention because of their unique rheological, mechanical, and thermal properties [4-6]. Catenated ring networks, or Olympic gels [7], have been developed with muscle-like properties [8] and reconfigurable topologies [9,10]. To understand the physics of catenated ring networks and hence engineer them for a desired application, a robust model system is required wherein topology can be tuned and studied at the single molecule level. Nature provides such a model system in the form of giant 2D catenated ring networks called kinetoplasts [11,12].

Kinetoplast DNA (kDNA) from trypanosomatid Crithidia fasciculata is a natural Olympic gel wherein approximately 5000 minicircles (\sim 2.5 kbp) and 25 maxicircles (\sim 40 kbp) are topologically interlocked in a quasi-2D plane [12]. The catenation valency of minicircles is approximately 3 [12–15]; however, the catenation valency of maxicircles is unknown. While the network of maxicircles and minicircles are

Published by the American Physical Society under the terms of the Creative Commons Attribution 4.0 International license. Further distribution of this work must maintain attribution to the author(s) and the published article's title, journal citation, and DOI.

interlocked with each other, each network can be sustained independently [16]. The nucleotide sequence of minicircles and maxicircles is different, and this property can be exploited to selectively digest maxicircles or minicircles in a controllable manner. Moreover, there are two different classes of minicircles, namely the major class and the minor class (accounting for $\sim 90\%$, and $\sim 10\%$ of the network, respectively), where each class is homogeneous in its base pair sequence but different from the other class [17]. There is currently no understanding of how these various classes of rings affect the kDNA conformation, polymer dynamics or mechanical properties.

Recently our group has studied various aspects of kDNA and proposed it as a model system for 2D catenated polymers [18–22]. For example, it has been shown that in response to constriction or electric field stretching, kDNA behave as an elastic sheet [18,19]. Its properties as a 2D polyelectrolyte have also been studied in response to the degree of confinement and ionic strength [20,21]. The unsatisfactory match of scaling laws based on a generalized Flory approach for a 2D polymer indicates that the physics of catenated polymers is yet to be fully realized. Furthermore, our group has demonstrated that the features of polymer-and-salt-induced phase transition of kDNA is quite different than that of linear DNA [22].

Herein we study the equilibrium size, shape, and relaxation spectrum of kDNA as a function of its molecular topology. A number of restriction enzymes were used to selectively remove the rings from the catenated network. Time-controlled digestion was also performed to randomly remove rings from the network to varying degrees in a controllable manner. Using this approach, we could selectively tune the topology of the kDNA while maintaining its overall molecular integrity, and thus generated a library of molecules with different topologies. Our results show that while topology has minimal

^{*}pdoyle@mit.edu

effects on the kDNA size and shape, it significantly affects the relaxation behavior owing to the mechanical strength of the kDNA network. We envision that this strategy can provide opportunities to selectively tune the physical properties of catenated DNA networks and shed light over the much debated physics of 2D polymers [23]. The results also provide rich information and guide the design of future 2D materials with specific properties.

II. MATERIALS AND METHODS

A. Sample preparation

Kinetoplasts (kDNA) from trypanosomatid Crithidia fasciculata were purchased from TopoGEN Inc. Received kDNA solution has a concentration of 612 µg/ml. The solvent was TE buffer, which is composed of 10 mM Tris-HCl, pH7.5, and 1 mM EDTA. For digestion experiments, different restriction enzymes (EcoRI-HF, PstI-HF and MluI, where HF refers to high fidelity) along with reaction buffer (rCutSmart) were purchased from New England Biolabs, Ipswich, MA. To digest minor class of minicircles (EcoRI-HF), maxicircles (PstI-HF) and combination of both (EcoRI-HF and PstI-HF) from the kDNA network 100 µl samples were prepared, which contains 2 µg of kDNA. Appropriate amounts of kDNA, enzymes and reaction buffer were mixed, and digestions were carried out for 2 h. For the digestion of major class of minicircles, time dependent reactions were carried out, and three different reaction times (5 min, 10 min, and 20 min) were chosen. All the reactions were carried out at 37°C and the enzymes were inactivated by heating the samples to 80°C for 20 min. Finally, the reaction buffer was replaced by 0.5X TBE buffer through four-times repeated centrifugation (5000 g, 2 min per run, at 20°C) and by using a 100 kDa cut-off membrane. After each run, the precipitate was topped up with 400 µl of 0.5X TBE-buffer. YOYO-1 fluorescence staining dye was purchased from Invitrogen, Carlsbad, CA. DNA was stained with intercalating dye YOYO-1 at a ratio of one dye molecule for each eight base pairs and kept at 4°C for overnight. The solution was prepared in 0.5X tris-boric acid-ethylenediaminetetraacetic acid (TBE) consisting of 0.687 µg/ml kinetoplasts. The oxygen scavenger β -mercaptoethanol (Sigma-Aldrich) was also added 4% (vol/vol) to prevent photobleaching.

B. Microfluidic chip fabrication

In this study, single molecule experiments were conducted in rectangular microfluidic channels with a height of $2\,\mu m$, a width of $40\,\mu m$ and a length of $1\,cm$. Microfluidic channels were fabricated by replication moulding in poly(dimethylsiloxane) (PDMS) of a patterned master stamp. Master silicon wafer containing features were patterned in SU8 using photolithography. After pouring the PDMS on the master stamp, it was cured by annealing at $65^{\circ}C$ overnight. The cured PDMS was removed from the master stamp and cut into individual chips and holes (4 mm diameter) were punched in each reservoir. The PDMS chips were cleaned by sonicating them for 10 minutes and soaking in 0.5X TBE buffer overnight to prevent permeation driven flow [24]. Glass cover slips were cleaned with ethanol and soaked at least 1

hour in 1 M NaOH. For experiments, a chip was taken out from buffer, washed with water, gently dried, and placed on a cleaned glass cover slip.

C. Fluorescence imaging

The solution containing the stained kinetoplast (kDNA) molecules was pipetted into two loading reservoirs connected by straight microchannel. The kDNA molecules were gently driven into channel by electrophoresis. For this purpose, two platinum wires connected to a voltage power supply (Trek Inc. model 677B) were immersed in the reservoirs. After bringing the molecules into the channel, the electric field was switched off and the molecules were allowed to relax to their equilibrium state for 2–5 minutes before image acquisition. kDNA molecules were imaged using a Zeiss Axiovert microscope equipped with a filtered light-emitting diode (ThorLabs M490L4) and a 63X oil immersion objective (numerical aperture 1.4). The filter set used was XF 100-3, which consists of an exciter filter 470 AF50 (central wavelength 470 nm, bandwidth 50 nm), dichroic filter 500DRLP, and emission filter 545AF75 (central wavelength 545 nm, bandwidth 75 nm). Movie clips capturing the individual kDNA molecules were recorded with a Photometrics 95B Prime sCMOS camera interfaced with a computer using Micro-Manager software. The image pixel size of $0.175 \times 0.175 \,\mu\text{m}^2$ was calibrated with the help of a metric ruler. The exposure time was kept 10 ms and an individual movie was recorded for 5000 frames with frame rates of 50 frames per second. For control and each enzyme digested sample, we measured and further analysed a pool of ~50 kDNA at the single-molecule level. Oversaturation of pixel intensity was avoided by careful adjustment of the camera gain and exposure time. Images were analysed using home-built scripts in MATLAB (MathWorks, Natick, MA).

III. RESULTS AND DISCUSSION

The heterogeneity in base pair sequencing of different classes of rings and the precise action of restriction enzymes have been harnessed to tune the topology of kDNAs. A summary of the experimental methodology is presented in Fig. 1. The restriction enzyme *EcoRI* has been used to cut the minor class of minicircles [17,25], *PstI* to cut the maxicircles [26], and a combination of *EcoRI* and *PstI* to cut both the minor class of minicircles and maxicircles. Next, we used *MluI* to digest the major class of minicircles as well as maxicircles [17] where fractional digestion of the network was controlled by digestion time. Single molecule experiments were conducted in straight microfluidic channels with a 2 μm height, 40 μm width, and a 1 cm length. Our prior papers [18,22] showed that this channel height orients kDNAs for ease of imaging and only moderately confines it.

Figure 2 presents a montage of fluorescence microscopy images of kDNAs. The ionic strength of the solution is 32.3 mM [20], which corresponds to a Debye length of 1.69 nm compared to the 2-nm bare width of dsDNA. Figure 2(a) shows representative images of control (pristine) kDNA and kDNA remodeled using various enzymes. The image displays a single frame (frame number 1137, chosen arbitrarily) out of 5000 frames recorded for each kDNA.

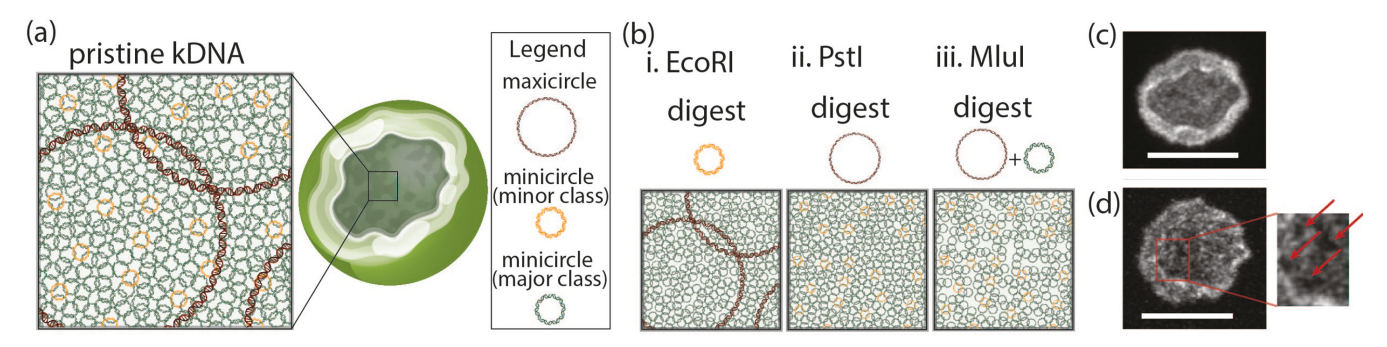


FIG. 1. Model schematic of the molecular topology of kinetoplasts and the experimental methodology to tune it. (a) Schematic diagram of a kinetoplast, a catenated 2D network (Olympic gel) made of thousands of interlocked rings of circular DNA. The average catenation valency of minicircles, irrespective of their class, is 3. However, the valency of maxicircles is not known. (b) With the precise action of restriction enzymes, either class or a combination of classes of rings can be removed from the network and, hence, tune the topology. (c) Super resolution confocal microscopy image showing the kinetoplast shape, which can be described as a wrinkled bowl with positive Gaussian curvature. (d) A representative molecule after digestion by the *MluI* enzyme for 10 minutes, where removal of maxicircles and a fraction of the major class of minicircles creates observable perforations within the network. Scale bar is 5 μm.

Each row displays the typical variability in shape and size of kDNA molecules. All the molecules have a nearly elliptical shape with a clearly identified outline. The brightness of the

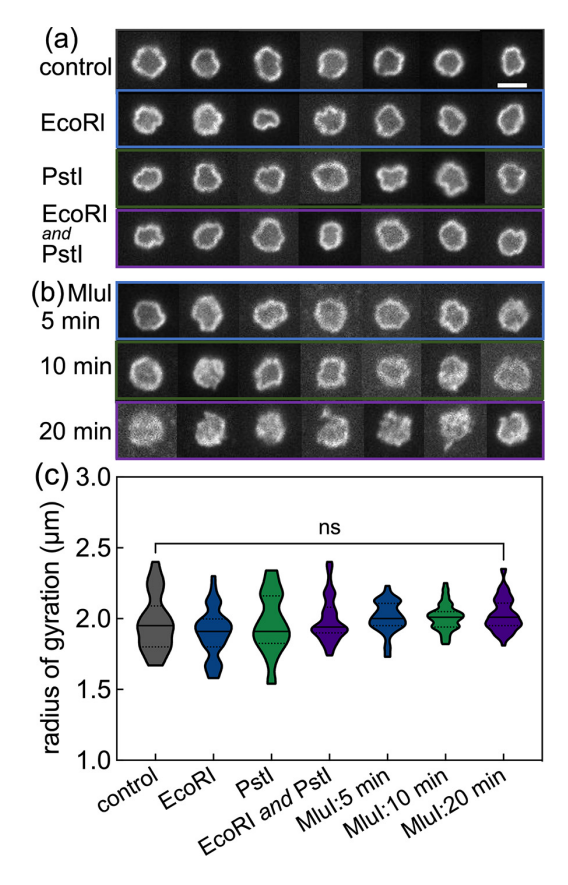


FIG. 2. Library of kinetoplasts molecules with different underlying topology and corresponding size distribution. [(a),(b)] Fluorescence microscopy images presenting the library of kDNAs corresponding to control and kDNAs remodelled with restriction enzymes. Each row displays the typical shape and size variability of molecules. (c) Violin plots of the size distribution of kDNAs corresponding to control and kDNAs remodelled with restriction enzymes. Scale bar is 5 μm .

outline is attributed to the dense fibril network of rings at the periphery of kDNAs [12]. This observation is consistent with previous study from our group [18,21]. These molecules have a topologically flat conformation with positive Gaussian curvature [22,27]. Interestingly, we observe qualitatively that there is no major difference in shape and size of the molecules after removal of the minor class of minicircles, the maxicircles, or a combination of both.

The influence of molecular topology was further quantified by measuring the radius of gyration (R_g) from the 2D projection of the fluorescence intensity of each kDNA, which maps kDNA's extension in a plane [19,22]. Here, R_g was determined as the square root of the trace of the radius of gyration tensor [28]. Violin plots, representing the distribution of $R_{\rm g}$, are presented in Fig. 2(c). Each violin plot maps the probability distribution of R_g , where the width of a plot corresponds to the frequency of the data points in each region. The central solid line represents the median, while dotted lines represent the ends of first and third quartiles. Statistical testing comparing the different distributions with the *control* gives p > 0.05, which implies that modifying kDNA topology by removing the minor class of minicircles and/or the maxicircles does not significantly influence its size. This nontrivial result implies, interestingly, that among the components of the kDNA network, it is the major class of the minicircles that plays the most important role in dictating the overall molecular size. This is also evidence that the catenated polymers offer great variability in their topology but very robust geometrical structure.

To investigate this result further, we chose to tune the amount of the major class of minicircles. While there is no enzyme, which can independently digest this type of ring, we used MluI, which digests both the major class of minicircles and the maxicircles. Representative images of molecules corresponding to different degrees of digestion, which is a function of digestion time, is shown in Fig. 2(b). Molecules corresponding to a digestion time of $\geqslant 10$ minutes show a change in shape compared to the control. For a reaction time of 20 minutes, below which molecular integrity is intact, significant visual deviation in shape of molecules can be seen. The R_g distributions are presented in Fig. 2(c). Again, with

TABLE I. Description of pristine (control) and digested networks. In the calculation of bending rigidity (κ), the viscosity of solvent ($\eta = 1$ centipoise) and radius of molecules ($r = 5 \mu m$) were used.

Enzyme used to remodel the network topology	Description of fractional digestion		Mean anisotropy	Ensemble average standard deviation of anisotropy (σ)	Bending rigidity $(\kappa) X k_B T$
Pristine (control)			0.868 ± 0.070	0.0165	54.7
EcoRI	~7% mass fraction of the total network	~7% mass fraction of the minicircles	0.883 ± 0.060	0.0177	52.6
PstI	~8% mass fraction of the total network		0.853 ± 0.066	0.0191	48.4
EcoRI and PstI	~ 14% mass fraction of the total network	~ 6% mass fraction of the minicircles	0.867 ± 0.062	0.0212	43.2
MluI for 5 min	~20% mass fraction of the total network	~12% mass fraction of the minicircles	0.867 ± 0.072	0.0254	38.7
MluI for 10 min	~25% mass fraction of the total network	~17% mass fraction of the minicircles	0.842 ± 0.060	0.0303	29.3
MluI for 20 min	~32% mass fraction of the total network	~24% mass fraction of the minicircles	0.839 ± 0.072	0.0407	23.6

regards to the molecular size of kDNA, statistical testing shows no significant difference in the $R_{\rm g}$ distribution. Another interesting featured is that we did not observe the crumpling of molecules even with the maximum digestion we could achieve while still maintaining the molecular integrity.

When referring to topology herein, we mean the nature of network manifold as a consequence of the fact that DNA rings within the molecular network cannot pass through one another nor could rearrange their relative spatial position as they are permanently interlocked by catenation with nearby rings (see Fig. 9). The topology of the pristine kDNA is known to be very complex [12–14,16,29] and bears a resemblance to chain-mail armor. Removing either class of rings from the network will change the nature of the network manifold and hence the topology in a nontrivial way.

Catenation valency is one of the most important parameters to quantify such a topology [12,13]. Based on the gel electrophoresis and electron microscopy data, which was rationalized using graph theory, Chen *et al.* [12,13] calculated the average catenation valency and the tiling pattern of the pristine kDNA network. The tiling pattern of the partially and randomly digested network cannot be deduced by their methodology. However, it is clear that the areal density of the rings is a measure of the average catenation valency. Thus we can calculate the average catenation valency of the digested network as, $v_d = v_p(1-f)$ (see Appendix C), where v_p and v_d are the catenation valency of the pristine and the digested network, respectively, and f is the fractional digestion of the minicircles (Table I). The calculated average valency of the minicircles is presented in Fig. 3.

Irrespective of their topology, kDNA molecules undergo small shape fluctuations (Movie S1 and S2) [30] and for a given environmental condition fluctuation in shape is stationary. Here, thermal fluctuation is measured in terms of variation in anisotropy as a function of time for individual molecules. The shape of a kDNA can be described as wrinkled bowl with an elliptical cross section [18]. Principle eigenvalues of the gyration tensor calculated from projected fluorescence intensity give length of the minor and major axes of the ellipse. The anisotropy then is defined as the ratio of minor axis and

major axis. The anisotropy measured in this way provides information about symmetry where a value of 1 represents circular conformation and a value of 0 a straight line. Hence, studying the temporal behavior of anisotropy not only provides the degree of thermal fluctuation but also the robustness/flexibility of the shape of the network manifold. The distribution of anisotropy for molecules in different samples are presented in Fig. 10. Although there is significant molecule-to-molecule variation in anisotropy within a sample, the average value for different samples remains almost same (p > 0.05). This also implies that the shape of the molecule does not change drastically by tuning its topology. The amplitude of fluctuation relative to its mean value, however, is significantly affected by tuning the topology. Variation in anisotropy as a function of time for quintessential molecules for the control and a MluI-digested molecule are presented in Fig. 4(a). The amplitude of anisotropy fluctuation for a given molecule is quantified in terms of the standard deviation of anisotropy (σ) over a given time series. It is clear that σ value increases after removing a fraction of rings from the

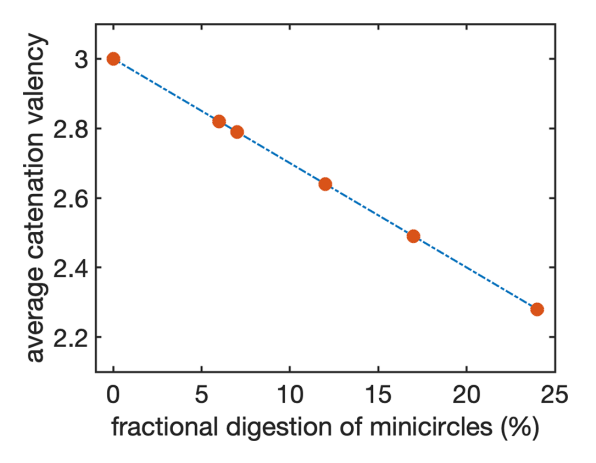


FIG. 3. Average catenation valency of the minicircles as a function of the fractional digestion of the minicircles. The catenation valency of the maxicircles is not known, hence the corresponding data has been omitted.

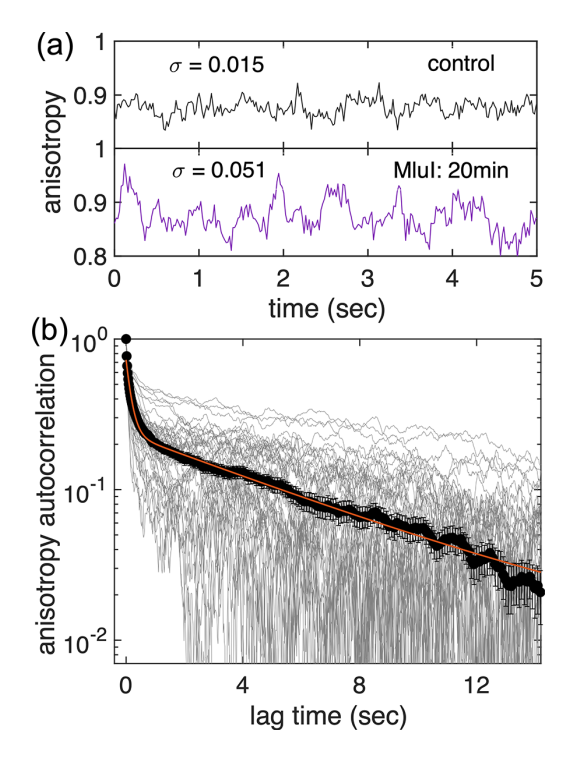


FIG. 4. (a) Upper panel shows the anisotropy fluctuation for control (pristine) kDNA and the bottom panel for a molecule digested with *MluI* for 20 min. Although the mean value of anisotropy remains almost the same (\sim 0.9), the standard deviation (σ) varies for different topologies. (b) Semilogarithmic plot of temporal autocorrelation function of anisotropy for the control molecules (N = 49) and their ensemble average (black).

network. The ensemble averaged values of σ calculated using equation (E1) for different samples are presented in Table I.

To study the dynamic behavior of the kDNA network we calculated the autocorrelation function $C(\tau)$ of the anisotropy A measured over T camera frames

$$C(\tau) = \frac{1}{\sigma^2 T} \sum_{t=1}^{T-\tau} (A(t) - \bar{A})(A(t+\tau) - \bar{A}), \qquad (1)$$

where σ^2 is the anisotropy variance and \bar{A} is the average value of anisotropy over a given time series. An ensemble of autocorrelation functions and their average for control

molecules is presented in Fig. 4(b). Qualitatively the autocorrelation for each molecule has a fast decay at short lag time followed by a tail at longer lag times. Accordingly, the ensemble average autocorrelation is fitted with the sum of two exponentials [Appendix F, Eq. (F1)]. The fast timescale (τ_1) was found to be 0.177 ± 0.018 s (SD), which is of the order of the relaxation timescale for the much smaller λ -DNA [28,31]. The characteristic timescale of the longer time tail (τ_2) was found to be 5.90 ± 0.81 s (SD).

Figure 5(a) presents the autocorrelation of anisotropy corresponding to the digestion of the minor class of minicircles or/and maxicircles. Inset of the figure shows a zoom in view of the autocorrelation for short lag times. It is clear that as rings are systematically removed from the network, the time constant for fast relaxation consequently increases. For the slower relaxation, however, the autocorrelation decreases relatively faster as we remove rings from the network, i.e., the time constant for slow relaxation decreases. Similar antagonistic trends between τ_1 and τ_2 but with more significant differences in magnitude are obtained for molecules after time-dependent digestion of rings using MluI [Fig. 5(b)].

The first time constant (τ_1) related to the faster decay of the autocorrelation function corresponds to a conformational decorrelation, i.e., time over which the network forgets its initial configuration. For a linear polymer, it also corresponds to the timescale over which a molecule diffuses a distance equivalent to its radius of gyration and is the relaxation time for the lowest mode in the Rouse model [32,33]. For free draining, the Rouse model considers the polymer as a set of beads connected by Gaussian springs and predicts the relaxation time as $\tau_1 = \zeta/k_{tot}$ where ζ is the total viscous drag on the chain and $k_{\text{tot}} (= k_B T / \Delta x^2)$ is the effective spring constant with Δx being the extension/contraction in Gaussian springs from its equilibrium size. k_BT is the thermal energy. Topologically 2D network of kDNA can be modelled as a 2D network of self-avoiding beads connected with Gaussian springs (see Fig. 11) [34,35]. Hydrodynamic interactions become decorrelated at length scales proportional to the channel height [36], accordingly the Rouse dynamics will dominate the shape fluctuations. Extending the Rouse formalism to 2D network it can be shown that $\tau_1 \sim \zeta \sigma^2/k_B T$ (see Appendix F).

The scaling of τ_1 with σ for molecules digested with two different classes of enzymes is shown in Fig. 12. The slopes of the regression line for two sets of samples are very close

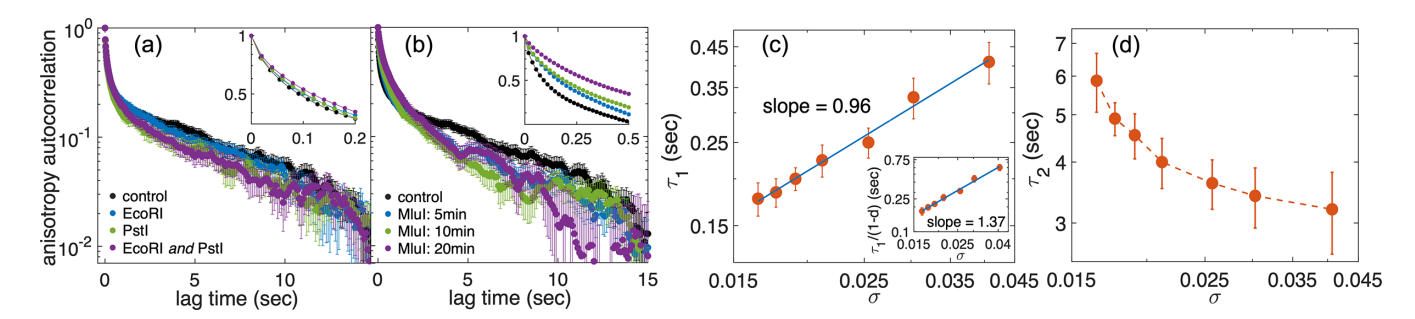


FIG. 5. Ensemble averaged time autocorrelation function of anisotropy (a) with well control removal of minicircles/maxicircles, (b) random removal of minicircles/maxicircles from the kDNA network. (c) Master curve (τ_1 vs σ) showing the universal nature of $\tau_1 \sim \sigma^{0.96\pm0.12}$. (d) τ_2 vs σ showing the monotonic decrease of τ_2 . Inset in (c) presents the influence of drag changing with degree of digestion (d) on scaling exponent.

and they fall onto a master plot with a universal scaling $(\tau_1 \sim \sigma^{0.96\pm0.12})$ [Fig. 5(c)]. The nature of this master plot implies that the scaling relation between τ_1 and σ is independent of detailed arrangements of rings and/or perforation within the catenated network. This observation is in accord with studies of perforated sheets wherein the crumpling critical temperature depends on the perforation area, but is independent of detailed arrangement of perforated holes within the sheet [37]. The relaxation time also encrypts the mechanical strength of the network. It has been shown that bending rigidity (κ) and relaxation time (τ_1) for vesicles are related as $\kappa = \eta r^3/\pi \tau_1$, where η is solvent viscosity and r is the equilibrium radius [38]. For a given η and r, $\kappa \sim \tau_1^{-1}$. Hence, removing rings softens the network. The calculated values of κ for different samples are listed in Table I.

The deviation from the Rouse prediction $(\tau_1 \sim \sigma^2)$ could be due to oversimplistic nature of the spring model of kDNA. While the size of the molecules remains invariant, the number of beads in the modelled network should reduce in proportion to the degree of digestion and hence the effective drag. Influence of digestion on effective drag is discussed in Appendix H. Inset in Figs. 5(c) and 13 show that when we account for this modification in drag, the scaling exponent increases to (1.37 - 1.52), which is still smaller than the Rouse prediction. It should also be noted that though there are many theoretical and simulation studies available about 2D polymers, [27,35,37,39–41] experimental results are scarce, and the prediction of the statistical models for 2D polymers has not been tested. To the best of our knowledge, this is the first experimental data presenting the universal scaling between two measured quantities for a 2D polymer.

The time constant (τ_2) associated with second mode of relaxation *decreases* [Fig. 5(d)] as we remove rings from the network, in contrast to τ_1 . This trend could not be rationalized by the spring model of the network in bulk. Our prior study on pristine kDNA conjectured that the longer time constant is the result of microfluidic confinement, which suppresses out-of-plane motion and can lead to long-lived local folds along the edge of the molecule [18]. Examples are shown in Fig. 15. The energy barrier of conformational fold transitions is related to κ , which decreases monotonically with fraction of digestion (Table I). The decline of κ will also weaken the sense of confinement for the molecules and facilitate out-of-plane motion. Together, these contributions lead to a reduction of τ_2 upon ring digestion.

IV. SUMMARY

In this study, we tuned the topology of a 2D catenated DNA network to understand its influence on equilibrium conformations and shape fluctuations. Although the molecular topology has minimal influence on the spatial extension of this 2D network, it significantly affects shape fluctuations. Remarkably, irrespective of details of the molecular topology, the relationship between the time constant of shape fluctuations and variance of shape anisotropy shows a universal scaling. Our results provide a route to selectively tune the physical properties of 2D catenated DNA networks and in doing so, we discovered unanticipated trends in properties related to

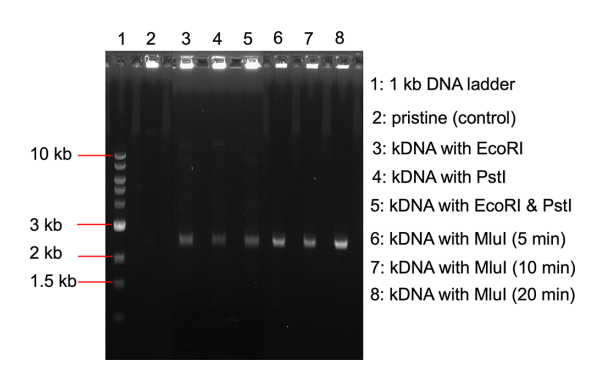


FIG. 6. Agarose gel electrophoresis showing the digestion of the kDNA network.

topological modifications, which will hopefully spurn further studies of this emergent class of polymers.

ACKNOWLEDGMENTS

This project was funded by NSF Grant CBET-1936696. We thank Dr. Cassandra Rogers of the W. M. Keck Facility for Biological Imaging at the Whitehead Institute for her support in confocal imaging.

APPENDIX A: AGAROSE GEL ELECTROPHORESIS

We characterized the digestion of the kDNA network by agarose gel electrophoresis. Samples were run on 0.8% agarose gel at room temperature in 1X TAE buffer at 150 V for 1.5 h. Figure 6 shows the bands for the samples corresponding to 1 kb ladder and digestion of kDNA network using different restriction enzymes. The first lane shows the band corresponding to 1 kb ladder with fragment sizes marked in kilobases (kb). The second lane shows the band corresponding to pristine (control) kDNA. Without any digestion, pristine kDNA molecules should remain in the well due to their large size (\sim 13 Mbp) as can be seen in lane 2. Lane 3 shows the sample corresponding to digestion using EcoRI, which digests the minor class of minicircles. Lane 4 corresponds to digestion using PstI, which digests maxicircles and lane 5 corresponds to digestion using a combination of (EcoRI and PstI), which digest the minor class of minicircles and maxicircles. Lanes 6, 7, and 8 correspond to digestion using MluI for 5, 10, and 20 minutes, respectively, which results in the digestion of maxicircles and the major class of minicircles to different degrees. We also calculated the fraction of digestion from the gel electrophoresis data. The extraction and purification of the kinetoplast DNA from gel bands was not possible as the yield for the digested bands was very low and the size of molecules inside the wells was very big and could not be easily extracted using a standard kit. Hence, we adopted an alternative method to calculate the fraction of digestion from the fluorescence intensity of the bands. Using ImageJ software, we calculate the intensity of each band. Under the assumption that the intensity is proportional to the concentration of the DNA, the digested fraction of the network was calculated and given in Table I.

It is well known that the enzyme activity decreases with time and the product formed follow a first-order exponential increase [42]. Our observation also suggests that the time dependent fractional digestion follows a standard first-

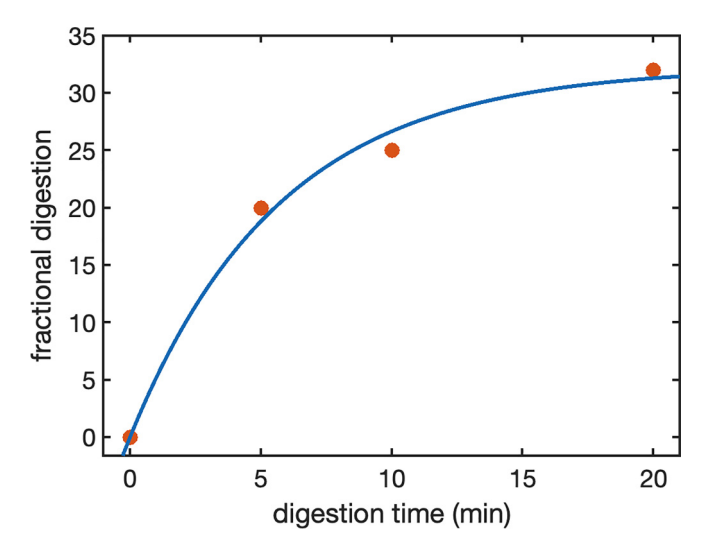


FIG. 7. Time-dependent fractional digestion of the kDNA network follows a standard first-order exponential increase. Red circles show the data points and the solid line is fit to $f(t) = a(1 - \exp(-kt))$.

order exponential increase $[f(t) = a(1 - \exp(-kt))]$, where $k = 0.175 \,\text{min}^{-1}$, t is the digestion time, and a = 32.3 is the maximum digestion (Fig. 7).

APPENDIX B: SUPER RESOLUTION LASER SCANNING MICROSCOPY

To understand the morphology of the kinetoplasts with different molecular topologies we imaged molecules using a super resolution laser scanning confocal microscope. A Zeiss LSM 980 with Airyscan 2 microscope was used in oil-immersion mode with a 63X objective (numerical aperture 1.4). Molecules were imaged in microfluidic channels with a height of 2 μ m as mentioned earlier. However, to minimize the motion of molecules for the best possible resolution, kDNA molecules were immersed in 77% glycerol. Stacks of images were collected and processed using Airyscan SR followed by the reconstruction of 3D images using ImageJ software.

Figure 8 presents a montage of super resolution confocal microscopy images. It can be seen that for *control* kDNA has a bowl-like (topologically two-dimensional) shape with the well-defined and relatively brighter periphery. As we remove rings from the network perforations are generated within the molecule, however, the overall shape is still bowl-like. Another interesting observation is that the rim of the molecule is relatively brighter, which could be due to a higher density of rings at the periphery.

APPENDIX C: TOPOLOGY OF THE KDNA NETWORK AND ITS QUANTIFICATION

When speaking of the topology of the kDNA network, we mean the nature of network manifold as a consequence of the fact that rings within kDNA network cannot pass through one another nor could rearrange their relative spatial position as they are locked by catenation with nearby rings. These catenations (constraints) are permanent (independent of time).

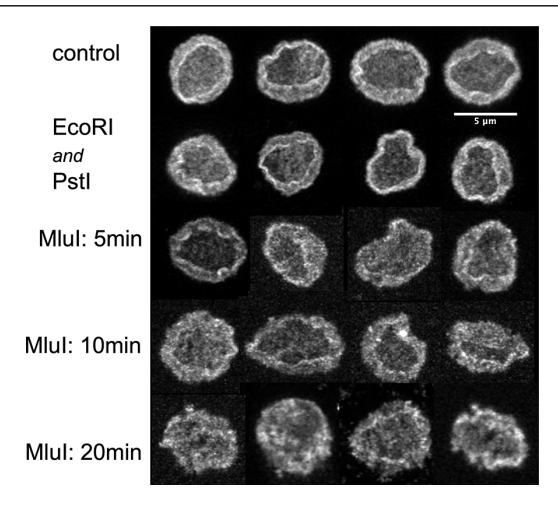


FIG. 8. Super resolution laser scanning fluorescence microscopy images of representative kDNA molecules for control and kDNA remodeled using different enzymes.

The topology of the pristine kDNA has been studied by many researchers [12–14,16,29] and it is well known that the network topology is very complex and bears a resemblance to chain-mail armor. The network is made of two types of rings, namely maxicircles and minicircles. While the network of maxicircles and minicircles are interlocked with each other, each network can be sustained independently [16]. Removing either class (maxicircles, minor class of minicircles, and major class of minicircles) of rings from the network will change the nature of the network manifold of pristine kDNA and hence the topology. For example, removing the maxicircles will change the network's topology in a nontrivial way. Prior to removal, we have two interpenetrating networks making a single manifold. However, after the removal of maxicircles, we will have just one network of minicircles within the manifold.

The catenation valency of the maxicircles is not known; however, the valency of minicircles is found to be approximately 3, i.e., each of the 5000 minicircles is intact and linked to an average of three neighbors [12,13,29]. Moreover, each minicircle is linked to its neighbors by a single interlock, i.e., Hopf link. Thus, based on the previous studies [12,13] and the catenation valency 3 of the minicircles, a simplified topology of the pristine kDNA network is presented in Fig. 9(a). After enzymatic digestion of minicircles, we could remove a fraction of DNA rings from the network randomly as shown in Fig. 9(b). The removal of the rings not only creates holes in the network but also changes the catenation valency of the minicircles, and hence the topology of the network in a nontrivial way.

Catenation valency is one of the most important parameters to quantify such a topology [13,29]. We calculated the change in catenation valency as a function of fractional digestion of the minicircles. Let N be the total number of minicircles, and A is the area of the pristine kDNA network. The average catenation valency ν_p of pristine network can be written as $\nu_p = \rho_p \pi R_g^2$, where $\rho_p = N/A$ is the number density of the minicircles and R_g is the radius of gyration of a minicircle. Now, under the assumption that the R_g of a minicircle, and the geometrical area of the network remain unchanged,

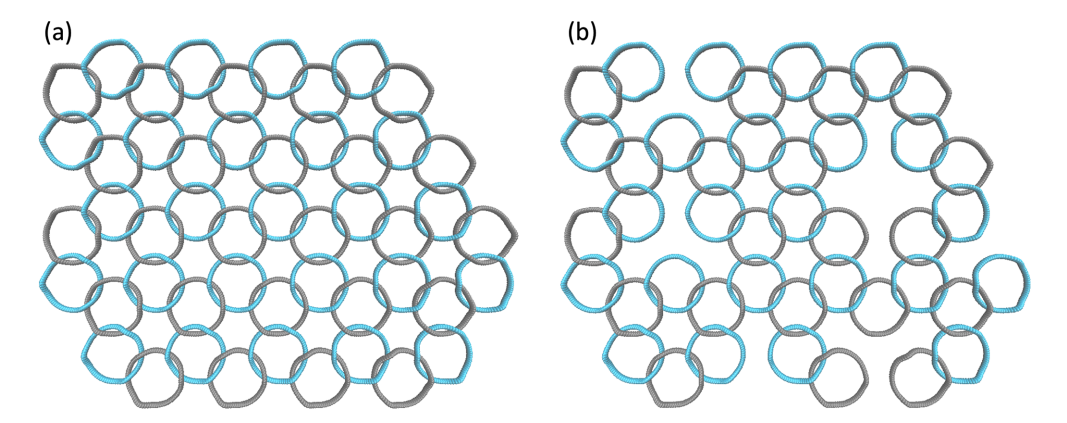


FIG. 9. The intrinsic topology of the kinetoplast network. (a) The topology of the pristine kDNA network is akin to chain-mail armor with the average catenation valency of rings within the network 3. (b) After removal of a fraction of the rings, the average catenation valency of the rings changes, and hence the topology of the network changes in a nontrivial way. Two colors of the rings are to guide the eye.

irrespective of rings digestion (Figs. 2 and 8), the average catenation valency of the digested network can be expressed as $v_d = v_p(1-f)$, where f is the fractional digestion of the minicircles as mentioned in Table I. The calculated average valency of the minicircles is presented in Fig. 3.

APPENDIX D: ANISOTROPY DISTRIBUTION

Mean of anisotropy for individual molecules has been obtained from the temporal series (5000 frames) and the distribution (Fig. 10) has been constructed over a population of about 50 molecules for each samples.

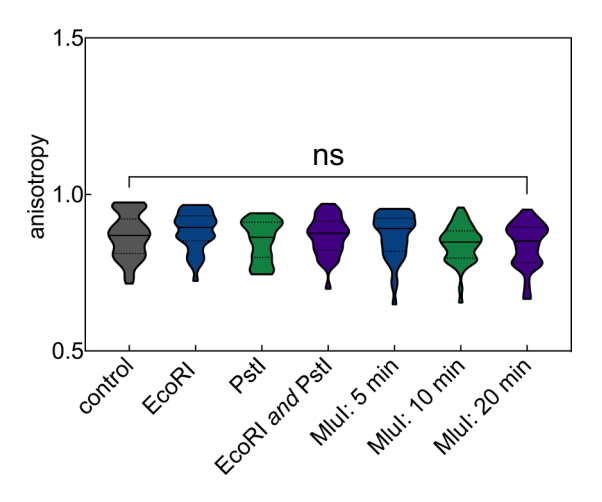


FIG. 10. Violin plots representing the anisotropy distribution of kinetoplasts corresponding to control and molecules remodelled using different restriction enzymes mention along the x axis below each distribution. The central solid line shows the median, while the dotted lines represent the ends of the first and third quartiles. Unpaired t-test with Welch's correction shows there is no significant (ns) (p > 0.05) difference in the distribution of MluI: 20 min digestion compared to control. Similar results have been found for all other distributions in between.

APPENDIX E: ENSEMBLE AVERAGE STANDARD DEVIATION OF ANISOTROPY

Anisotropy fluctuation of an individual molecule for a recorded time series presents a distribution, and hence corresponding mean and standard deviation can be calculated. Ensemble averaged standard deviation (σ) of the standard deviations of the various distributions for a sample can be calculated as follows:

$$\sigma = \sqrt{\left(\sigma_1^2 + \sigma_2^2 + \sigma_3^3 + \dots + \sigma_n^2\right)/n},$$
 (E1)

where σ_n is the standard deviation of the *n*th distribution and *n* is total number of distributions. Here time series variation of anisotropy for each molecule represents a distribution and the number of molecules constitute the number of distribution (*n*) for a sample. The values are given in Table I.

APPENDIX F: ANISOTROPY AUTOCORRELATION AND RELAXATION TIME

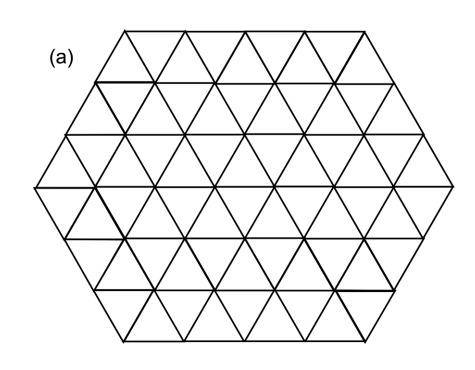
The autocorrelation function of anisotropy was fitted as the summation of two exponentials using the following equation:

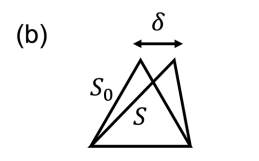
$$C(\tau) = \alpha + \beta \exp(-t/\tau_1) + \gamma \exp(-t/\tau_2), \quad (F1)$$

where τ_1 and τ_2 represent the time constants related to first and second mode of relaxation, respectively, and α is the infinite time correlation (ideally 0). We fitted the data from the first point at nonzero time to the point after which the data appears to fall towards zero superexponentially (14.2 s for control). We used the Levenberg-Marquardt algorithm, incorporating the standard error on each point as a weighting. For control, fitting gives $\tau_1 = 0.177 \pm 0.018 \, \text{sec}$ (SD), $\tau_2 = 5.90 \pm 0.81 \, \text{sec}$ (SD), with $\alpha = 0.0080 \pm 0.0113$ (SD), (SD, standard deviation). Similar procedures have been used to fit the autocorrelation function for other samples.

The relaxation time τ_1 is related to the thermal fluctuation of the kinetoplast and τ_2 is associated with the influence of confinement, as shown in our prior study.

The relaxation τ_1 of the fast mode of kinetoplast is analogous to lowest mode relaxation of the linear polymers. We could consider the kinetoplast as a network of two-dimensional (2D) self-avoiding beads connected with





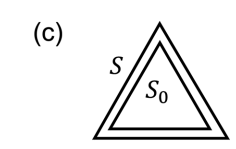


FIG. 11. (a) 2D network of springs with sixfold coordination. Deformation mode of a triangular network, (b) shear mode, and (c) compression mode

Gaussian springs [Fig. 11(a)], thus under the paradigm of the Rouse dynamics [32], the relaxation time (τ_1) can be represented as

$$\tau_1 = \zeta / k_{2D}, \tag{F2}$$

where ζ is the total viscous drag and can be written as

$$\zeta = \xi L^2 \tag{F3}$$

with ξ representing the drag for an individual bead and L is the linear extension of the network compared to the size of individual spring, i.e., $L = L_0/b$, where L_0 is absolute linear extension and b is the size of a spring. k_{2D} is the effective spring constant of the network.

At our experimental condition, we have calculated the autocorrelation of anisotropy (A = x/y), where x and y are the minor and major axis of the ellipse and map the linear extension (L) of the kinetoplast network. The fluctuation in anisotropy (dA), which can be mapped in the standard deviation of anisotropy (σ) measurements, can be expressed as

$$dA = dx/y - (x/y^2)dy,$$
 (F4)

$$\sigma \sim dA = dx/y - (x^2/y^2)dy/x.$$
 (F5)

Here dx and dy represent the fluctuation in the minor and major axis, where x and y represent the average over course of measurement and can be considered constants.

In a spring model of the polymer, the relation between thermal energy and force constant is actually related to the fluctuation in polymer length (fluctuation in length is proportional to the length of the polymer as it can be thought of as the series of springs). Under the assumption that the fluctuations along the x and y directions are orthogonal and independent; $\sigma \sim \sigma_x \sim \sigma_y$ i.e.,

$$\sigma \sim dx/y$$
. (F6)

Now applying the equipartition theorem, and relating the thermal energy with the spring energy

$$k_{2D} \sim k_B T / dx^2, \tag{F7}$$

$$k_{2D} \sim k_B T / \sigma^2$$
. (F8)

Here, k_{2D} is the effective spring constant of the network. Hence the Rouse relaxation (thermal relaxation τ_1) for kinetoplast (2D network) is related to standard deviation of anisotropy σ as

$$\tau_1 \sim \zeta \sigma^2 / k_B T$$
. (F9)

An alternative way to obtain the relation between the first relaxation time and anisotropy is considering the network of spring (Fig. 11) with sixfold connectivity kept at temperature T where each spring has an unstretched length of S_0 . The corresponding potential energy can be written as [43]

$$V_{sp} = 1/2[k_{sp}(S - S_0)^2],$$
 (F10)

where k_{sp} is the force constant of individual spring and S is the instantaneous length of the spring under the influence of thermal energy k_BT . Deformation of the network can happen in two modes, shear [Fig. 11(b)] and compression [Fig. 11(c)]. We will consider here the shear mode: Figure 11(b) shows that under the influence of shear, the top vertex moves by δ along the positive x axis, thus left-hand spring gets elongated by $\delta/2$ and the right-hand spring gets shortened by $\delta/2$, approximately. Since there is no change in the bottom spring, the total change in potential energy per vertex is

$$\Delta U \cong k_{sp} \delta^2 / 4. \tag{F11}$$

Now, we consider the probability of displacement from equilibrium, $\delta \sim S - S_0$, is proportional to Boltzmann factor $\exp(-\Delta U/k_BT)$. Hence, the mean square value of δ is given as

$$\langle \delta^2 \rangle = \frac{\int_{-\infty}^{+\infty} \delta^2 \exp(-k_{sp} \delta^2 / 4k_B T) d\delta}{\int_{-\infty}^{+\infty} \exp(-k_{sp} \delta^2 / 4k_B T) d\delta},$$
 (F12)

$$\langle \delta^2 \rangle \sim k_B T / k_{sp}.$$
 (F13)

In this model, $\langle \delta^2 \rangle$ maps the mean square anisotropy fluctuation of the unit triangle in the network.

The network of spring with effective spring constant $(k_{2D} \sim k_{sp})$ is embedded in the viscous medium at temperature T, and has mean square anisotropy fluctuation $(\langle \sigma^2 \rangle \sim \langle \delta^2 \rangle)$, thus lowest mode relaxation time of the network can be expressed as

$$\tau_1 = \zeta / k_{2D},\tag{F14}$$

$$\tau_1 \sim \zeta \sigma^2 / k_B T.$$
 (F15)

APPENDIX G: MASTER CURVE AND UNIVERSAL SCALING

Figure 12 shows the scaling relation between anisotropy and relaxation times for two different sets of samples: first where digestion is sequence controlled (I and II) and second where digestion is mainly time controlled (III and IV). The slopes for σ versus τ_1 are very close which indeed supports the universal scaling mentioned in Fig. 5. The different slopes and poor fitting of the data, in the case of τ_2 versus σ for two sets of digestion indicates that τ_2 decreases monotonically with σ , but does not follow a universal scaling. The possible mechanism responsible for the τ_2 is discussed in detail in Appendix I.

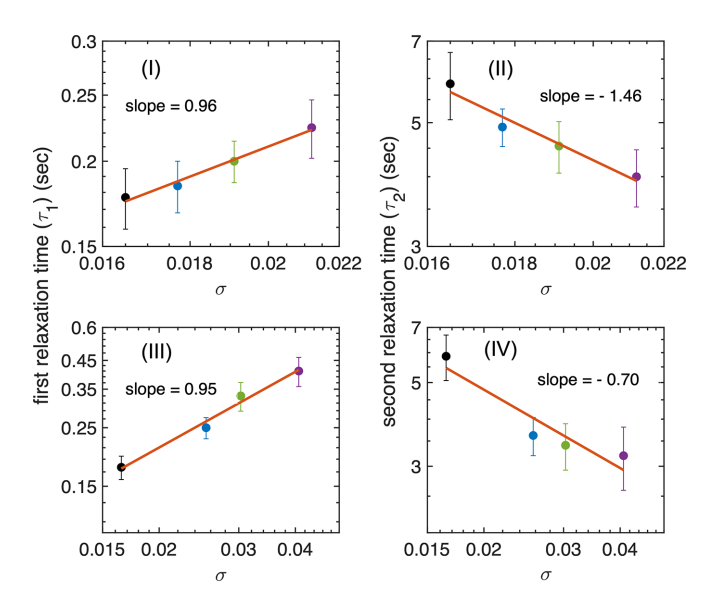


FIG. 12. Linear regression of σ vs τ_1 and τ_2 for molecules remodelled using different enzymes. Top panels (I and II) for control, and corresponding to enzymes EcoRI, PstI, and (EcoRI and PstI) and the bottom panels (III and IV) corresponding to MluI for different temporal digestion. Slopes for the scaling of τ_1 vs σ are very close and independent of the nature of enzymes used, hence follow the universal scaling. Different values of slopes of the data suggest that the τ_2 vs σ does not follow a universal scaling.

APPENDIX H: INFLUENCE OF FRACTIONAL REMOVAL OF RINGS ON EFFECTIVE DRAG OF NETWORK

In the Rouse model, the effective drag is proportional to the number of rings within the network. The relation between the drag of digested molecules $(\tilde{\zeta})$ with respect to pristine (ζ) can be written as

$$\tilde{\zeta} = \zeta(1 - d),\tag{H1}$$

where d is the total fractional digestion of the network (values are listed in Table I). Incorporating this change in drag into equation (F15) yields

$$\tau_1 \sim \zeta (1 - d) \sigma^2 / k_B T.$$
 (H2)

In Fig. 13 we plot $\tau_1/(1-d)$ versus σ . The scaling for data incorporating the influence of drag gives a slope of 1.37. A similar analysis for only sequence-controlled digestion (initial four data points) gives a slope of 1.52. The underestimation of scaling compared to the Rouse prediction (slope = 2) could be, among other reasons, due to the underestimation of the digested fraction of the network. There is also a possibility that the Rouse model cannot be directly implemented in 2D polymers. We have also presented the scaling of τ_1 versus molecular weight of the network (as a function of the fractional digestion) in Fig. 14.

APPENDIX I: INFLUENCE OF CONFORMATIONAL TRANSITION ON τ_2

In prior study [18], we conjecture that the longer time constant is the result of microfluidic confinement. The

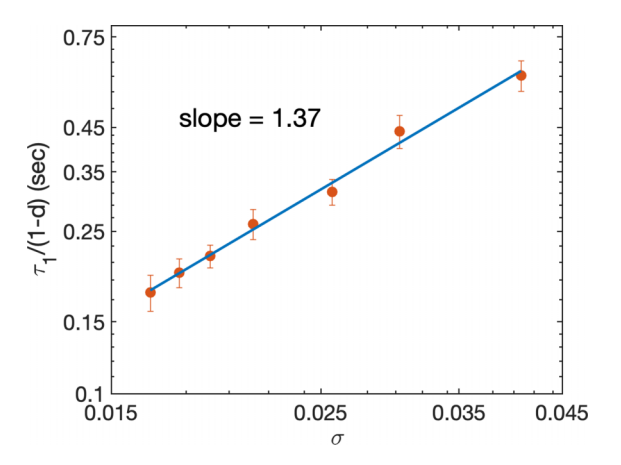


FIG. 13. Linear regression showing the scaling relation of $\tau_1/(1-d)$ vs σ .

kinetoplasts are moderately confined inside microfluidic channel, which facilitates their imaging for longer periods of time; however, it suppresses out-of-plane motion, which could induce the apparent correlation at longer lag time. Interaction of kinetoplast with walls could also lead to the conformational transition of molecules during measurements, which leads to the long-time correlation of anisotropy. One such example for *control* is shown in Fig. 15(a) where a molecule shows a particularly strong conformational transition (folding) event. After the folding event, the anisotropy increases significantly and the autocorrelation for such full set of data has a long time tail with τ_2 value of 20 ± 1 sec. The autocorrelation function measured from two subsets of the data, i.e., before and after folding, decays relatively much faster. The τ_2 values using these two subsets of data are 4.2 ± 0.2 sec and 4.8 ± 0.2 sec.

Such conformational transition has a high-energy barrier and is related to the bending rigidity of the network. As shown in Table I, the bending rigidity of the network decreases monotonically with fraction of digested DNA, accordingly the energy barrier of the conformational transition decreases. One such example after the removal of the maxicircles and minor class of minicircles using *EcoRI* and *PstI* is shown

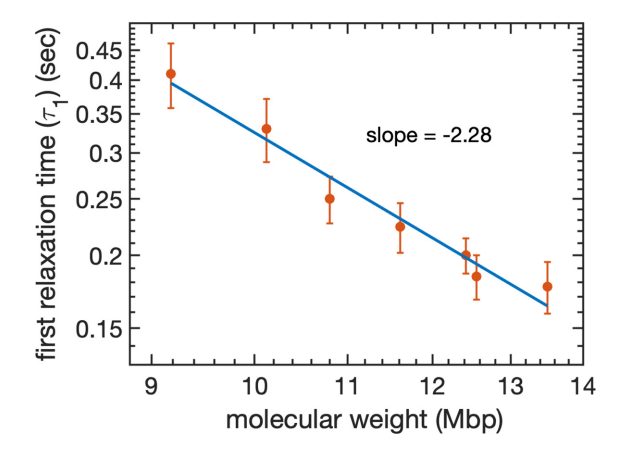


FIG. 14. Linear regression showing the scaling relation of τ_1 vs molecular weight of the kDNA network presented in Mega base pairs (Mbp). 1 bp = 650 daltons.

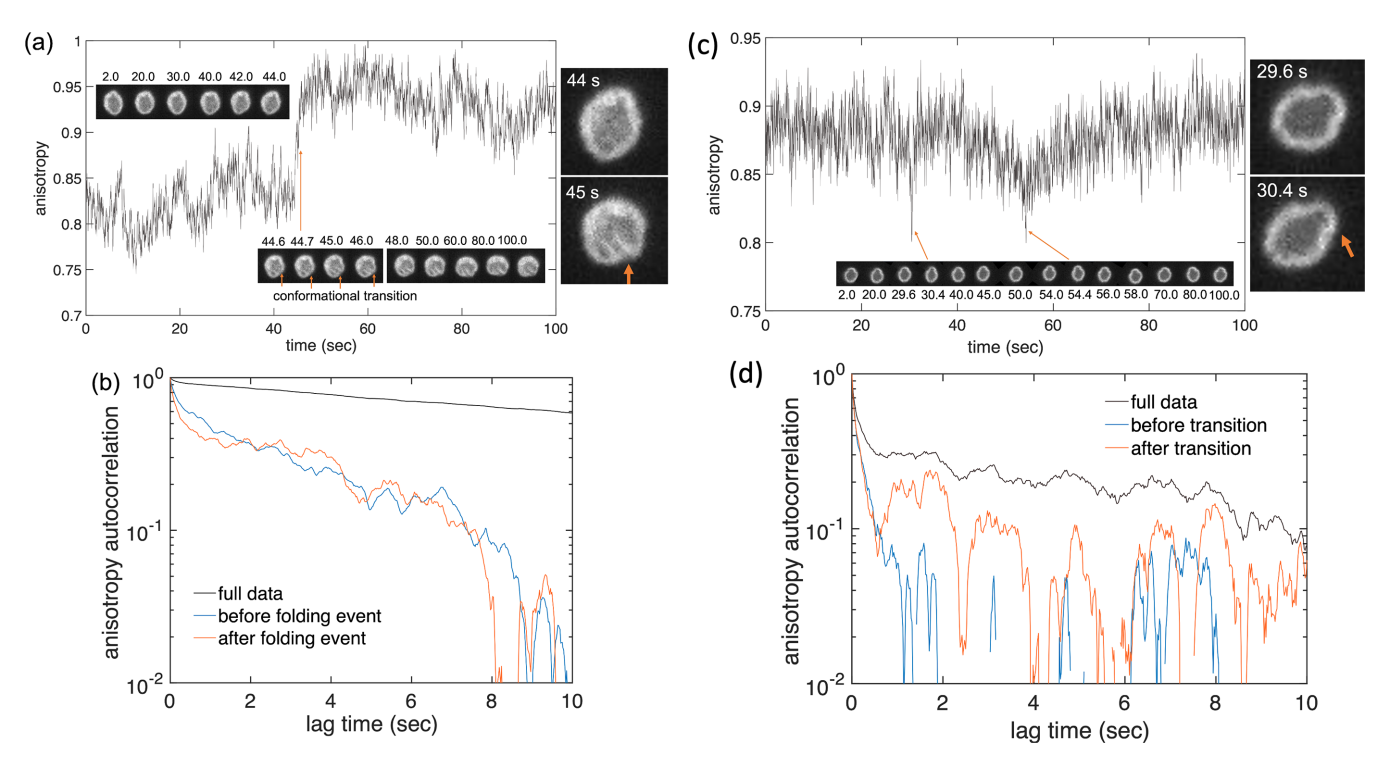


FIG. 15. (a) The anisotropy of a kinetoplast for the control sample that undergoes a folding event. As marked by arrows, the edge folds inwards spontaneously and molecules remain arrested in that conformation, which leads to a significant increment of anisotropy. (b) The autocorrelation function of the anisotropy for molecule is shown in (a). The autocorrelations corresponding to anisotropy fluctuations before and after the folding event decay much faster when the transitional periods (40-60 sec) is excluded. (c) The anisotropy of a kinetoplast for the *EcoRI and PstI* sample that undergoes a transient folding event. As marked by arrows the edge get elongated and anisotropy decreases, which leads to decrease of anisotropy. (d) The autocorrelation function of the anisotropy for molecule shown in (c). The autocorrelations [before and after folding event (\sim 55 sec)] decay relatively faster when the transitional period (45-65 sec) is excluded from the analysis.

in Fig. 15(b). As reflected in anisotropy, the molecule shows both sharp (\sim 30.4 sec) and gradual (\sim 54.4 sec) conformational transitions. However, it does not spend a long time in any specific state and this behavior is reflected in the autocorrelation with τ_2 value of 6.7 \pm 1 sec, much smaller than the control kDNA. When we calculate the autocorrelation function before and after the gradual conformational transition, we see that the autocorrelation decays even faster. The τ_2

values using these two subsets of data are 0.7 ± 0.1 sec and 1.3 ± 0.2 sec.

Thus, we postulate that the trend of τ_2 decreasing with increasing digestion is related to the change in network rigidity, which allows the molecule to more easily execute the out-of-plane motion. Furthermore, abrupt folding transitions no longer become long lived as the network softens with an increasing degree of digestion.

^[1] D. M. Wulstein, K. E. Regan, J. Garamella, R. J. McGorty, and R. M. Robertson-Anderson, Topology-dependent anomalous dynamics of ring and linear DNA are sensitive to cytoskeleton crosslinking, Sci. Adv. 5, eaay5912 (2019).

^[2] B. W. Soh, A. R. Klotz, R. M. Robertson-Anderson, and P. S. Doyle, Long-Lived Self-Entanglements in Ring Polymers, Phys. Rev. Lett. 123, 048002 (2019).

^[3] M. D. Frank-Kamenetski and A. V. Vologodski, Topological aspects of the physics of polymers: The theory and its biophysical applications, Sov. Phys. Usp. **24**, 679 (1981).

^[4] L. F. Hart, J. E. Hertzog, P. M. Rauscher, B. W. Rawe, M. M. Tranquilli, and S. J. Rowan, Material properties and applications of mechanically interlocked polymers, Nat. Rev. Mater. 6, 508 (2021).

^[5] G. Liu, P. M. Rauscher, B. W. Rawe, M. M. Tranquilli, and S. J. Rowan, Polycatenanes: Synthesis, characterization, and physical understanding, Chem. Soc. Rev. 51, 4928 (2022).

^[6] M. Lang, J. Fischer, M. Werner, and J.-U. Sommer, Swelling of Olympic Gels, Phys. Rev. Lett. 112, 238001 (2014).

^[7] E. Raphaël, C. Gay, and P. G. De Gennes, Progressive construction of an "Olympic" gel, J. Stat. Phys. **89**, 111 (1997).

^[8] P. Hu, J. Madsen, Q. Huang, and A. L. Skov, Elastomers without covalent cross-linking: Concatenated rings giving rise to elasticity, ACS Macro Letters 9, 1458 (2020).

^[9] Y. S. Kim, B. Kundukad, A. Allahverdi, L. Nordensköld, P. S. Doyle, and J. R. Van Der Maarel, Gelation of the genome by topoisomerase II targeting anticancer agents, Soft Matter 9, 1656 (2013).

- [10] B. A. Krajina, A. Zhu, S. C. Heilshorn, and A. J. Spakowitz, Active DNA Olympic Hydrogels Driven by Topoisomerase Activity, Phys. Rev. Lett. 121, 148001 (2018).
- [11] T. A. Shapiro and P. T. Englund, The structure and replication of kinetoplast DNA, Annu. Rev. Microbiol. **49**, 117 (1995).
- [12] J. Chen, C. A. Rauch, J. H. White, P. T. Englund, and N. R. Cozzarelli, The topology of the kinetoplast DNA network, Cell 80, 61 (1995).
- [13] J. Chen, P. T. Englund, and N. R. Cozzarelli, Changes in network topology during the replication of kinetoplast DNA, EMBO J. 14, 6339 (1995).
- [14] D. Michieletto, D. Marenduzzo, and E. Orlandini, Is the kine-toplast DNA a percolating network of linked rings at its critical point?, Phys. Biol. **12**, 036001 (2015).
- [15] L. Ibrahim, P. Liu, M. Klingbeil, Y. Diao, and J. Arsuaga, Estimating properties of kinetoplast DNA by fragmentation reactions, J. Phys. A: Math. Theor. 52, 034001 (2019).
- [16] T. A. Shapiro, Kinetoplast DNA maxicircles: Networks within networks, Proc. Natl. Acad. Sci. USA 90, 7809 (1993).
- [17] L. Birkenmeyer, H. Sugisaki, and D. S. Ray, The majority of minicircle DNA in *Crithidia fasciculat* strain CF-Cl is of a single class with nearly homogeneous DNA sequence, Nucleic Acids Res. 13, 7107 (1985).
- [18] A. R. Klotz, B. W. Soh, and P. S. Doyle, Equilibrium structure and deformation response of 2D kinetoplast sheets, Proc. Natl. Acad. Sci. USA 117, 121 (2020).
- [19] B. W. Soh and P. S. Doyle, Deformation response of catenated DNA networks in a planar elongational field, ACS Macro Lett. 9, 944 (2020).
- [20] B. W. Soh, A. Khorshid, D. Al Sulaiman, and P. S. Doyle, Ionic effects on the equilibrium conformation of catenated DNA networks, Macromolecules 53, 8502 (2020).
- [21] B. W. Soh and P. S. Doyle, Equilibrium Conformation of Catenated DNA Networks in Slitlike Confinement, ACS Macro Lett. 10, 880 (2021).
- [22] I. Yadav, D. Al Sulaiman, B. W. Soh, and P. S. Doyle, Phase transition of catenated DNA networks in poly(ethylene glycol) solutions, ACS Macro Lett. **10**, 1429 (2021).
- [23] A. D. Schlüter, P. Payamyar, and H. C. Öttinger, How the world changes by going from one- to two-dimensional polymers in solution, Macromol. Rapid Commun. 37, 1638 (2016).
- [24] G. C. Randall and P. S. Doyle, Permeation-driven flow in poly(dimethylsiloxane) microfluidic devices, Proc. Natl. Acad. Sci. USA 102, 10813 (2005).
- [25] J. H. J. Hoeijmakers, B. Schoutsen, and P. Borst, Kinetoplast DNA in the insect trypanosomes *Crithidia lucilae* and *Crithidia fasciculata*, Plasmid 7, 199 (1982).
- [26] L. R. Carpenter and P. T. Englund, Kinetoplast maxicircle DNA replication in *Crithidia fasciculata* and *Trypanosoma brucei*, Mol. Cell. Biol. 15, 6794 (1995).

- [27] J. M. Polson, E. J. Garcia, and A. R. Klotz, Flatness and intrinsic curvature of linked-ring membranes, Soft Matter 17, 10505 (2021).
- [28] C. C. Hsieh, A. Balducci, and P. S. Doyle, An experimental study of DNA rotational relaxation time in nanoslits, Macromolecules **40**, 5196 (2007).
- [29] P. He, A. J. Katan, L. Tubiana, C. Dekker, and D. Michieletto, Single-molecule structure and topology of kinetoplast DNA networks, arXiv:2209.01293.
- [30] See Supplemental Material at http://link.aps.org/supplemental/ 10.1103/PhysRevResearch.5.013141 for movies presenting the shape fluctuation of kinetoplast molecule due to thermal energy.
- [31] W. Reisner, K. J. Morton, R. Riehn, Y. M. Wang, Z. Yu, M. Rosen, J. C. Sturm, S. Y. Chou, E. Frey, and R. H. Austin, Statics And Dynamics Of Single DNA Molecules Confined In Nanochannels, Phys. Rev. Lett. 94, 196101 (2005).
- [32] M. Doi and S. F. Edwards, The Theory of Polymer Dynamics (Oxford University Press, New York, 1988).
- [33] I. Yadav, W. Rosencrans, R. Basak, J. A. van Kan, and J. R. C. van der Maarel, Intramolecular dynamics of dsDNA confined to a quasi-one-dimensional nanochannel, Phys. Rev. Res. 2, 013294 (2020).
- [34] Y. Kantor, M. Kardar, and D. R. Nelson, Statistical Mechanics of Tethered Surfaces, Phys. Rev. Lett. 57, 791 (1986).
- [35] Y. Kantor and D. R. Nelson, Crumpling Transition in Polymerized Membranes, Phys. Rev. Lett. 58, 2774 (1987).
- [36] J. J. Jones, J. R. C. van der Maarel, and P. S. Doyle, Intrachain Dynamics Of Large dsDNA Confined To Slitlike Channels, Phys. Rev. Lett. **110**, 068101 (2013).
- [37] D. Yllanes, S. S. Bhabesh, D. R. Nelson, and M. J. Bowick, Thermal crumpling of perforated two-dimensional sheets, Nat. Commun. 8, 1381 (2017).
- [38] H. Zhou, B. B. Gabilondo, W. Losert, and W. van de Water, Stretching and relaxation of vesicles, Phys. Rev. E 83, 011905 (2011).
- [39] W. Helfrich, Elastic properties of lipid bilayers: Theory and possible experiments, Z. Naturforsch, 28, 693 (1973).
- [40] M. Plischke and D. Boal, Absence of a crumpling transition in strongly self-avoiding tethered membranes, Phys. Rev. A 38, 4943 (1988).
- [41] M. J. Bowick, A. Cacciuto, G. Thorleifsson, and A. Travesset, Universality classes of self-avoiding fixed-connectivity membranes, Eur. Phys. J. E 5, 149 (2001).
- [42] A. G. Marangoni, Characterization of enzyme activity, *in* Enzyme Kinetics: A Modern Approach (John Wiley, Hoboken, NJ, 2002).
- [43] D. Boal and D. H. Boal, Mechanics of the Cell (Cambridge University Press, Cambridge, 2012).